Quantum confinement in phosphorus-doped silicon nanocrystals

Dmitriy V. Melnikov and James R. Chelikowsky
Department of Chemical Engineering and Materials Science,
Minnesota Supercomputing Institute,
University of Minnesota, Minneapolis, MN 55455

(Dated: February 16, 2004)

Abstract

Electronic properties of phosphorus donors in hydrogenated silicon nanocrystals are investigated using a real space *ab initio* pseudopotential method for systems with up to 500 atoms. We present calculations for the ionization energy, binding energy, and electron density associated with the doped nanocrystal. We find that the ionization energy for the nanocrystal is virtually *independent of size*. This behavior may be attributed to localization of the electron around the impurity site owing to a large electron-impurity interaction within confined systems. In contrast to this result, the calculated hyperfine splitting exhibits a *strong size dependence*. For small nanocrystals it greatly exceeds the bulk value. This finding agrees with recent experimental measurements.

PACS numbers:

Electronic and optical properties of semiconductor nanostructures are strongly affected by quantum confinement due to the reduced dimensionality of these systems [1]. In nanocrystals or quantum dots, where the motion of electrons (or holes) is limited in all three dimensions, quantum confinement results in a strong increase of the optical excitation energies when compared to the bulk. One expects that other electronic and optical properties will be affected as well. For example, in bulk semiconductors, shallow donors (or acceptors) are crucial in determining the transport properties required to construct electronic devices. However, these properties are expected to be significantly altered in highly confined systems such as quantum dots. Important questions arise as to whether dopants will continue to play a role similar to that in bulk semiconductors and whether new applications such as quantum computation [2] will become possible.

Experimental studies of shallow impurities in quantum dots, such as P in Si nanocrystals, have been slow to address such issues. In part, this is due to difficulties in preparation of samples in a controllable manner; it is hard to ensure that a quantum dot contains only one impurity. For such reasons, only a few experimental studies have focused on doping of quantum dots. These studies have utilized photoluminescence and electron spin resonance measurements, most of which have been performed on silicon dots. Increasing the dopant concentration results in distinct changes in photoluminescence properties such as suppression of the signal [3] and a blue-shift of photoluminescence maxima with decreasing particle size in heavily *p*-doped porous silicon [4]. From these measurements, it is not clear whether or not the doping of Si nanocrystals provides a generation of free charge carriers [4, 5]. Electron spin resonance involves measuring the hyperfine splitting (HFS) of the defect electron levels, which is directly related to localization of the dopant electron density on the impurity site [6]. In Si nanocrystals with radii of 10 nm doped with P, a hyperfine splitting of 110 G has been observed [7]. This splitting is in sharp contrast to the bulk value of 42 G. However, the intensity of the signal was very small compared to the conduction electron signal. A size dependence of the HFS was also found for Si quantum dots with radii around 50 nm [8], although in this case it was probably influenced by an asymmetrical shape of Si crystallites.

Recently, a strong size dependence of the HFS of P atoms was observed in much smaller nanocrystallites with radii of 2 - 3 nm [9].

Theoretical studies of shallow impurities in quantum dots have also lagged relative to calculations for pure, undoped systems. The large number of atoms and low symmetry have hindered such studies. To date, only empirical studies have been performed for impurities in quantum dots [10–12]. These calculations involve the utilization of various parameters, which are usually assumed to have bulk-like values. Another common drawback in these past studies is the use of a generic hydrogen-like potential to model the impurity atom.

Here, we use a real-space, *ab initio* pseudopotential density functional method [13] to examine the electronic properties of a single phosphorus impurity in a hydrogenated Si quantum dot containing hundreds of atoms. The nanocrystals were modeled as spherical, bulk-terminated Si clusters whose surface is passivated by hydrogen atoms. For doped dots, one silicon atom is substituted by a phosphorus atom. We model P, Si and H atoms using *ab initio* Troullier-Martins pseudopotentials [14]. Cut-off radii for s, p, and d components of the P pseudopotential were chosen to be 1.85 a.u (1 a.u.=0.529 Å). Parameters for the Si and H pseudopotentials and other technical details are given elsewhere [13].

We carefully tested convergence of the results with respect to the real-space grid spacing. We found that reasonably converged results (*e.g.*, a total energy converged within $\sim$0.05 eV) could be obtained with a grid spacing of 0.65 a.u. for systems with P atoms and 0.9 a.u. for pure Si nanocrystals. This difference in grid spacing stems from the “hard” nature of the P pseudopotential. The real space domain of calculations was taken to be 8 - 10 a.u. larger than the radius of the dot. The Kohn-Sham equations were solved self-consistently in this domain. The boundary condition for solving the Hartree potential was set by a multipole expansion for the charge density [13]. Typically, about 10 iterations were necessary for convergence in phosphorus-doped dots; pure Si dots converged faster. We examined several geometries for the P atom within the dot *i.e.*, a P placed at the center of the dot, off center, and on the surface. We found no significant relaxations of surrounding Si atoms. The largest change in position occurred when the P was positioned off center. In this case, the P atom was shifted by about 0.1 a.u. in the outward direction.

In contrast to supercell approaches, our real space method allows us to consider energy differences between charged clusters in a straightforward manner [13]. We calculated ionization energies I_d for P-doped nanocrystals and affinity energies A_p for pure Si nanocrystals using charged systems:

$$I_d = E(n-1) - E(n), \tag{1}$$

$$A_p = E(n) - E(n+1), \tag{2}$$

where E is the ground state total energy of the $n-$, $(n+1)-$ and $(n-1)-$electron systems. The binding energy E_B for the donor electron can be calculated as a difference between these two quantities:

$$E_B = I_d - A_p. \tag{3}$$

This definition of the binding energy E_B corresponds to two separate processes: First, the doped dot is ionized, *i.e.* the electron is physically removed from the nanocrystal and I_d is determined. Then, it is added to a dot of equivalent size without an impurity atom being present, and A_p is calculated. A similar approach was utilized in tight-binding calculations [12]. This definition of the binding energy for the donor atom can be contrasted with that for a bulk system, where the binding energy is defined as the difference between the dopant electron level and conduction band continuum. In nanocrystals or quantum dots, such a definition is problematic since an electron being excited into an unoccupied state (below the vacuum level) will be confined by the physical size of the dot and will continue to interact strongly with the impurity atom.

The calculated ionization, affinity and binding energy as a function of quantum dot radius R are shown in Fig. 1. The ionization energies for pure hydrogenated Si nanocrystals are also given for comparison. We note that ionization and affinity energies for pure Si quantum dots have values close to those calculated recently for hydrogenated Ge nanocrystals [15]. The most surprising feature in Fig. 1a is that the ionization energy I_d shows virtually no dependence on the size of the dot. It assumes the bulk value of approximately 4.2 eV [16] even for nanoscale systems.

The peculiar dependence of $I_d(R)$ is dramatically different from the behavior of the ionization energy in Si quantum dots where this quantity is very large at small radii and gradually decreases, scaling as $R^{-1.1}$, to its bulk value. Although this dependence of the ionization energy on radius is weaker than R^{-2} law predicted by effective mass theory [17], it is, nevertheless, a consequence of spatial confinement of electrons (holes) in quantum dots. It is surprising that this behavior is absent in the functional dependence of $I_d(R)$. The binding energy E_B, which scales as $R^{-0.8}$, is shown in Fig. 1b. These values are close to results of the tight-binding method [12], even though the ionization energy has a constant value in this range of sizes. We also plot in Fig. 1b the dependence of the ”band gap”, *i.e.* the difference between the lowest level with single occupancy and the highest doubly occupied level, in P-doped systems. This quantity is blue-shifted with respect to the bulk values where it should be approximately equal to the Si band gap. Comparison with results for pure hydrogenated Si dots [18] of the same radius shows that it is smaller by about 10% than values of the HOMO-LUMO gaps. The large values of the binding energy suggest that for dots in this size regime, the donors cannot be considered as shallow. This is largely due to the weak screening present in quantum dots and the physical confinement of the donor electron within the dot.

The nature of the Si-P bond can be clarified by examining the charge density of the dopant electron $|\Psi(r)|^2$ for several dot sizes. In Figure 2, we illustrate the charge profile for the case when the impurity is at the dot center. The density is plotted along the [100] direction; results in other directions are similar. At all dot radii, the dopant wave function is strongly localized around the impurity site, *i.e.*, the majority of the charge is within the P-Si bond length. From effective mass calculations [17], it follows that the envelope wave function of the dopant electron is given by $j_0(\pi r/R) \propto \sin(\pi r/R)/r$. Our calculated charge profile (Figure 2) is at variance with this description. This difference in the spatial distributions can be attributed to the weaker screening in quantum dots. At these sizes, the dielectric constant is several times smaller than the bulk value [18, 19], giving rise to the increase of the effective electron-impurity potential and stronger localization of the electron around the defect atom.

Given the charge distribution of the dopant electron, one can evaluate the isotropic hyperfine parameter and the corresponding HFS, which determines the contact interaction between the electron and defect nuclei. We utilized the method of Van de Walle and Blöchl [20] to extract the isotropic hyperfine parameter and the resulting HFS. Our calculated hyperfine splittings for a P atom positioned in the dot center are given in Figure 3. At small sizes, the HFS is very large owing to strong localization of the electron around the impurity. As the radius increases, the value of the splitting decreases. Our calculated results scale with radius R of the dot as $R^{-1.5}$ (effective mass theory gives R^{-3}). In Figure 3, we also present the experimental data of Ref. [9]. The measured values of the HFS falls on the best fit to calculated results. Computational limitations prevent us from comparing directly to the experimental size regime. Even though our dots are smaller than those studied experimentally, in both cases the effective Bohr radii extracted from the wave-functions are significantly smaller than the bulk effective Bohr radius of 16.7 Å. This indicates that dopant electron properties are affected by quantum confinement at all sizes.

Our results are not strongly dependent on the choice of the P site. We examined other sites by replacing one of Si atoms in each shell with a P atom while retaining the passivating hydrogen atoms. We found that the ionization and binding energies were unchanged to within ∼5 %, independent of the impurity atom position; the behavior of binding energy is similar to the corresponding result of Ref. [12]. The value of the HFS also remains largely unchanged, save for the outermost layers of the dot. This behavior is demonstrated in Figure 4, where the HFS is plotted as a function of defect position in a representative dot $Si_{86}H_{76}P$. Near the surface, the P atom electron density becomes more delocalized and the HFS shows a notable decrease in value from the value when P resides in the dot center. However, the surface position is energetically unstable with respect to the interior sites, *i.e.*, we found the center site for the P atom to be more stable by 0.61 eV relative to the surface site. Neglecting the surface site and the outer layers, the HFS varies by only ∼10% over the interior sites. As such, it would be difficult to use the experimental value to establish which sites are likely, save to rule out the surface layer.

In summary, we have performed a study of the properties of hydrogenated Si quantum dots doped with a single phosphorus atom. We calculated the ionization energy and binding energy of the defect. Surprisingly, the ionization energy does not exhibit behavior characteristic of quantum confinement; the defect ionization energy remains constant throughout the range of sizes studied and equal to the ionization energy of bulk silicon. The charge density associated with the excess dopant electron shows a strong localization towards the impurity site in small dots, and it starts to delocalize when the radius increases. This may be attributed to weak screening in quantum dots resulting in the strong electron-impurity interaction. From our calculated charge density, we evaluated the isotropic hyperfine parameter and the HFS for our phosphorus-doped nanocrystals. We found that the HFS is large in small systems and decreases with size, in close agreement with recent experimental findings.

We are grateful to W. B. Fowler for helpful discussions. We also acknowledge support for this work by the National Science Foundation, the Computational Materials Science Network of the United States Department of Energy, and the Minnesota Supercomputing Institute. This work was supported in part by the Army High Performance Computing Research Center (AHPCRC) under the auspices of the Department of Army, Army Research Laboratory (ARL) under Cooperative Agreement number DAAD19-01-2-0014. The content of which does not necessarily reflect the position or the policy of the government, no official endorsement should be inferred.

---

[1] A.D. Yoffe, Adv. Phys. **50**, 1 (2001).

[2] B.E. Kane, Nature **393**, 133 (1998); D.P. DiVincenzo, Nature **393**, 113 (1998).

[3] A. Mimura, M. Fujii, Sh. Hayashi, D. Kovalev, and F. Koch, Phys. Rev. B **62**, 12625 (2000).

[4] G. Mauckner, W. Rebitzer, K. Thonke, and R. Sauer, Solid state Comm. **91**, 717 (1994).

[5] D. Kovalev, H. Heckler, G. Polisski, and F. Koch, Phys. Status Solidi B **215**, 871 (1999).

[6] G. Feher, Phys. Rev. **114**, 1219 (1959).

[7] J. Müller, F. Finger, R. Carius, and H. Wagner, Phys. Rev. B **60**, 11666 (1999).

[8] B.J. Pawlak, T. Gregorkiewicz, C.A.J. Ammerlaan, W. Takkenberg, F.D. Tichelaar, and P.F.A. Alkemade, Phys. Rev. B **64**, 115308 (2001)

[9] M. Fujii, A. Mimura, Sh. Hayashi, Y. Yamamoto, and K. Murakami, Phys. Rev. Lett. **89**, 206805 (2002).

[10] C.-Y. Fong, H. Zhong, B.M. Klein, and J.S. Nelson, Phys. Rev. B **49**, 7466 (1994).

[11] I.-H. Lee, K.-H. Ahn, Y.-H. Kim, R.M. Martin, and J.-P. Leburton, Phys. Rev. B **60**, 13720 (1999).

[12] M. Lannoo, C. Delerue, and G. Allan, Phys. Rev. Lett. **74**, 3415 (1995).

[13] J.R. Chelikowsky, J. Phys. D: Appl. Phys. **33**, R33 (2000).

[14] N. Troullier and J.L. Martins, Phys. Rev. **B43**, 1993 (1991); L. Kleinman and D.M. Bylander, Phys. Rev. Lett. **48**, 1425 (1982).

[15] D.V. Melnikov, and J.R. Chelikowsky, unpublished.

[16] M. Schluter, J.R. Chelikowsky, S.G. Louie, and M.L. Cohen, Phys. Rev. Lett. **34**, 1385 (1975).

[17] L. E. Brus, J. Chem. Phys. **79**, 5566 (1983); *ibid* **79**, 4403 (1983).

[18] S. Ögüt, J.R. Chelikowsky, and S. Louie, Phys. Rev. Lett. **79**, 1770 (1997).

[19] S. Ögüt, R. Burdick, Y.Saad, and J.R. Chelikowsky, Phys. Rev. Lett., to be published.

[20] C.G. Van de Walle, P.E. Blöchl, Phys. Rev. B **47**, 4244 (1993).

Figure Captions

FIGURE 1. (a) Ionization energy I_d for phosphorus-doped nanocrystal (▼) and electron affinity A_p (▲) as a function of nanocrystal's radius R. Ionization energy for pure hydrogenated Si nanocrystals (■) is also shown. Solid lines are the best fits to calculated points, the dotted line is a guide to an eye. (b) Binding energy E_B (■) and the energy difference between the defect level with single occupancy and the highest occupied state with double occupancy (□) as a function of the dot's radius.

FIGURE 2. Charge density for the dopant electron along [100] direction. x is coordinate along that direction, and arrows indicate the radius of the dot.

FIGURE 3. Calculated (•) and experimental (▲) hyperfine splitting (HFS) versus the radius R of the quantum dot. The solid line is the best fit to our calculations (a bulk value of the HFS 42 G was used to obtain this fit). The inset shows experimental data of Ref. [9] together with the fit to results of the calculations. Two sets of experimental points correspond to the average size of nanocrystals (×) and the size of nanocrystals (▲) estimated from comparison of photoluminescence energies for doped and undoped samples (see Ref. [9])

FIGURE 4. Calculated hyperfine splitting in $\mathrm{Si}_{86}\mathrm{H}_{76}\mathrm{P}$ quantum dot as a function of the normalized position r_0/R of the P atom in the quantum dot whose radius is R. The dotted line is the average value of the HFS.

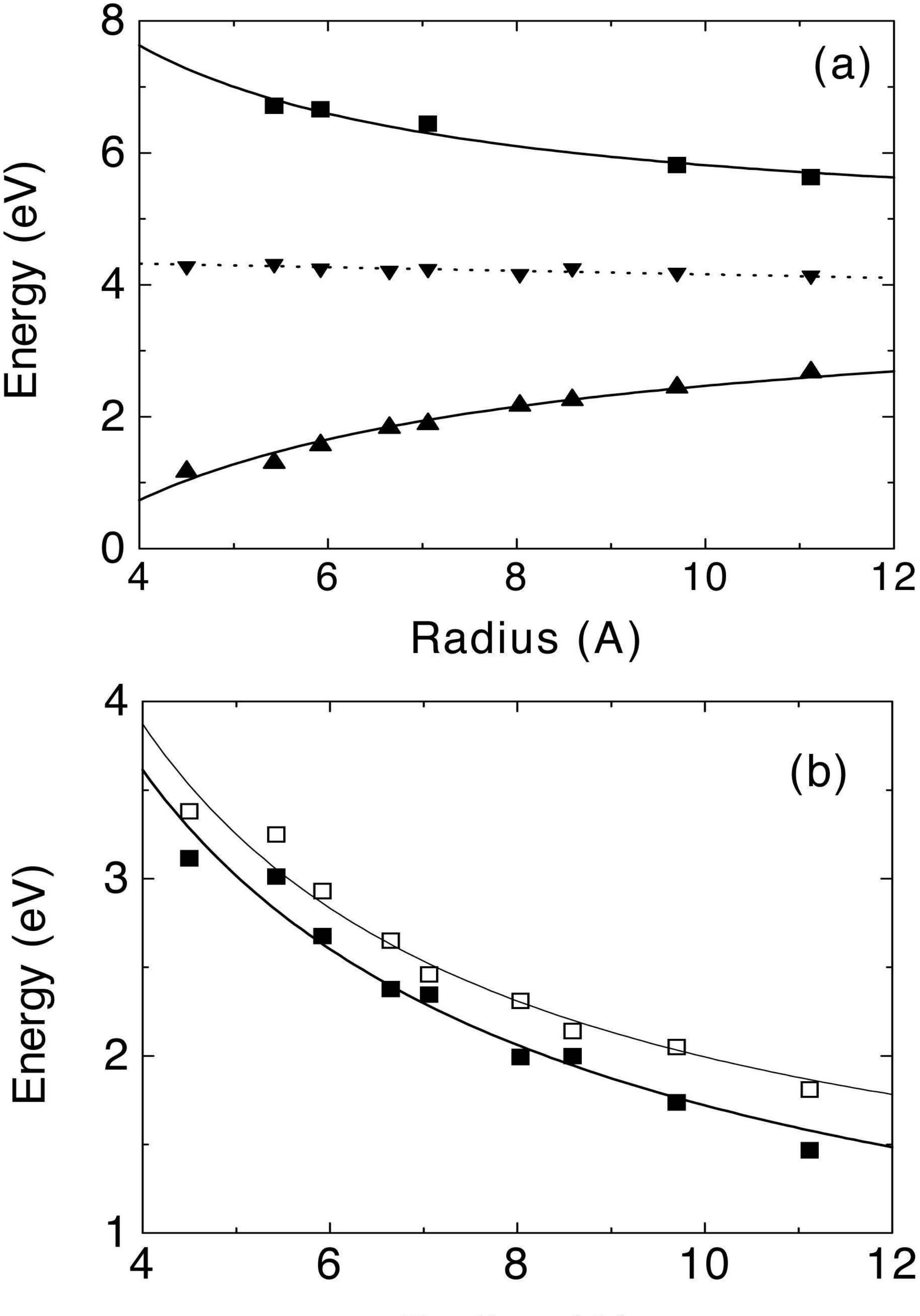
(a)
Energy (eV)
0
2
4
6
8
Radius (A)
4
6
8
10
12
(b)
Energy (eV)
1
2
3
4
Radius (A)
4
6
8
10
12

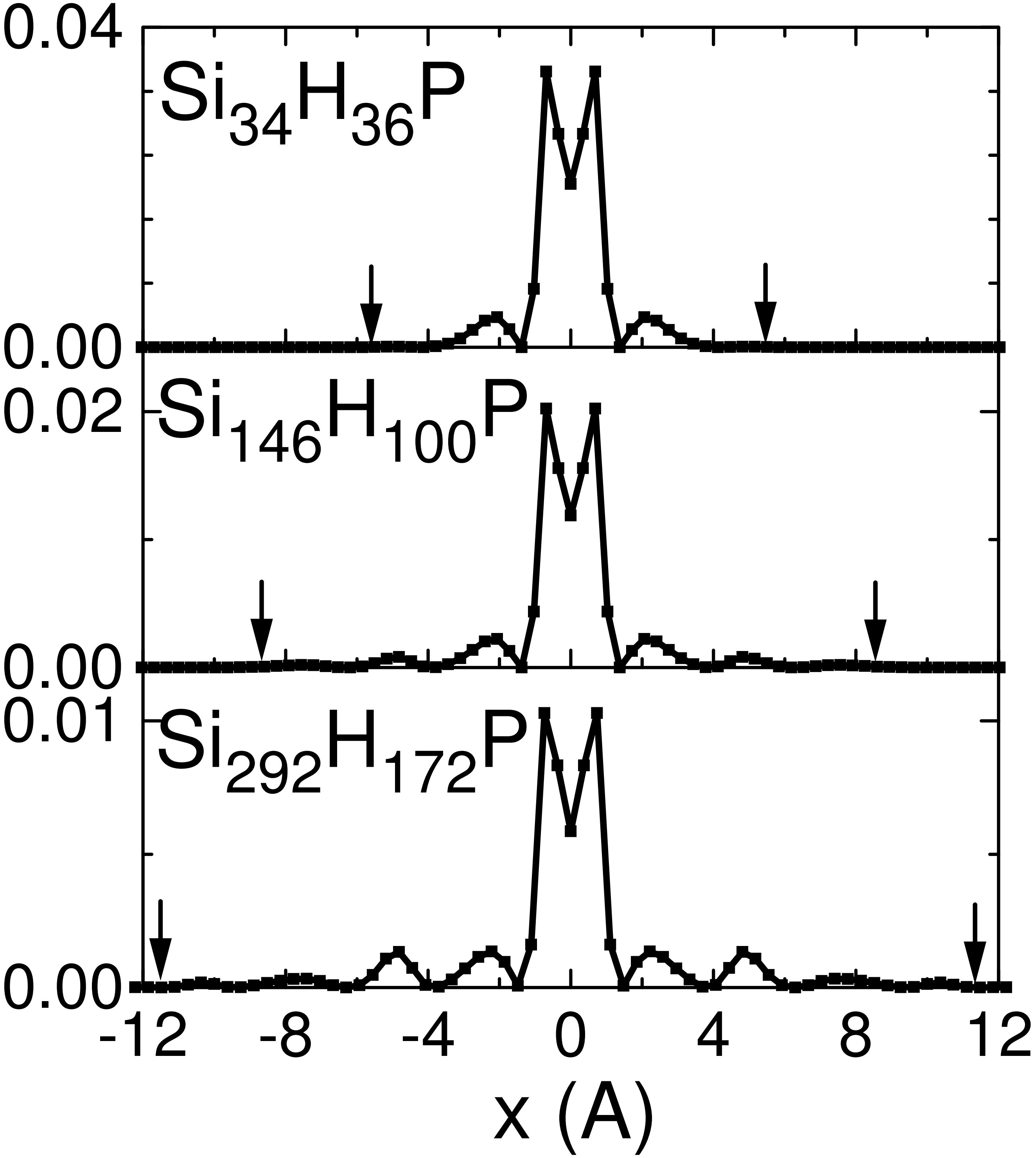
0.04
0.00
0.02
0.00
0.01
0.00
-12
-8
-4
0
4
8
12
x (A)
$|\Psi(x)|^2$ (A^{-3})
$Si_{34}H_{36}P$
$Si_{146}H_{100}P$
$Si_{292}H_{172}P$

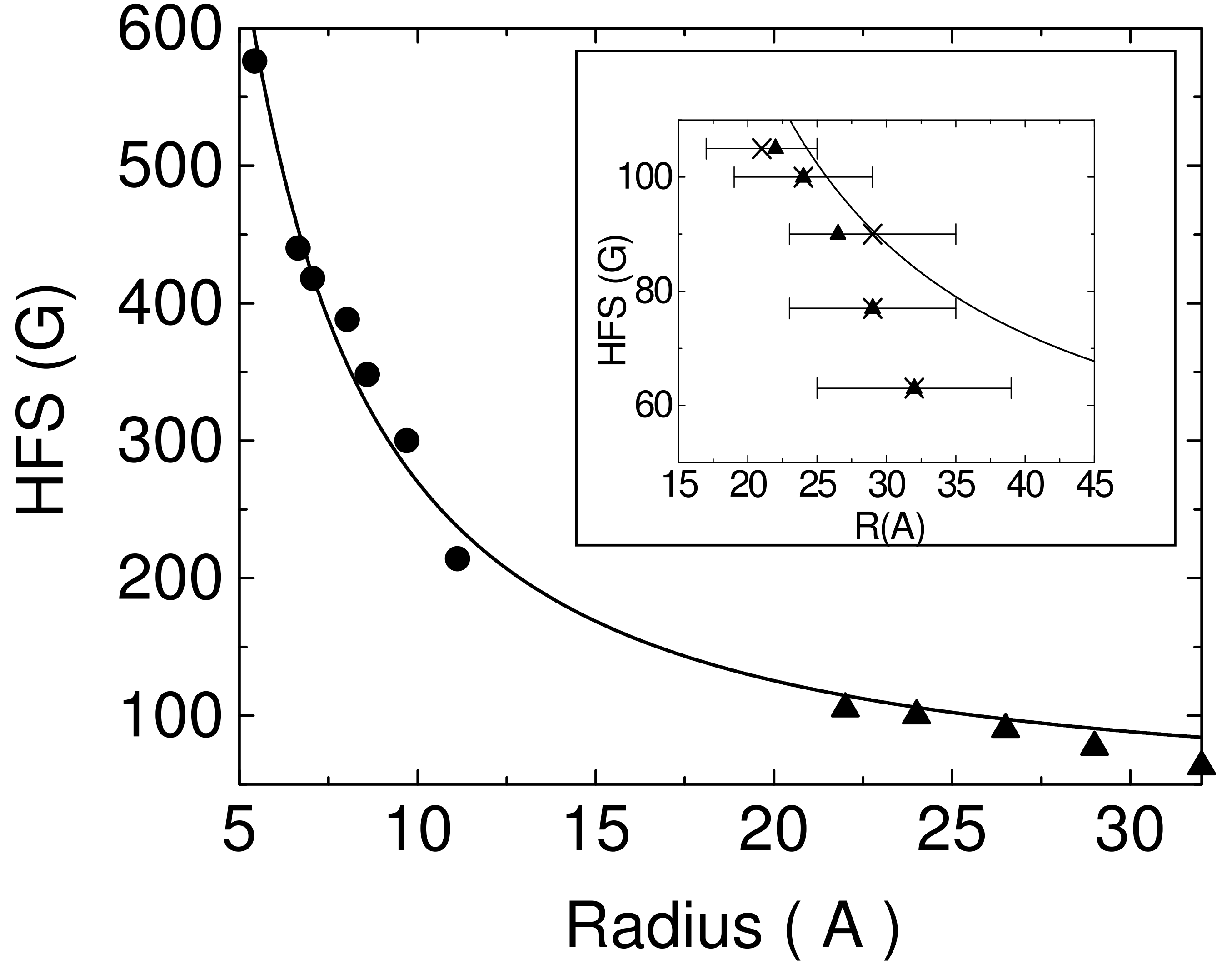

600
500
400
300
200
100
HFS (G)
5
10
15
20
25
30
Radius (A)
100
80
60
HFS (G)
15
20
25
30
35
40
45
R(A)

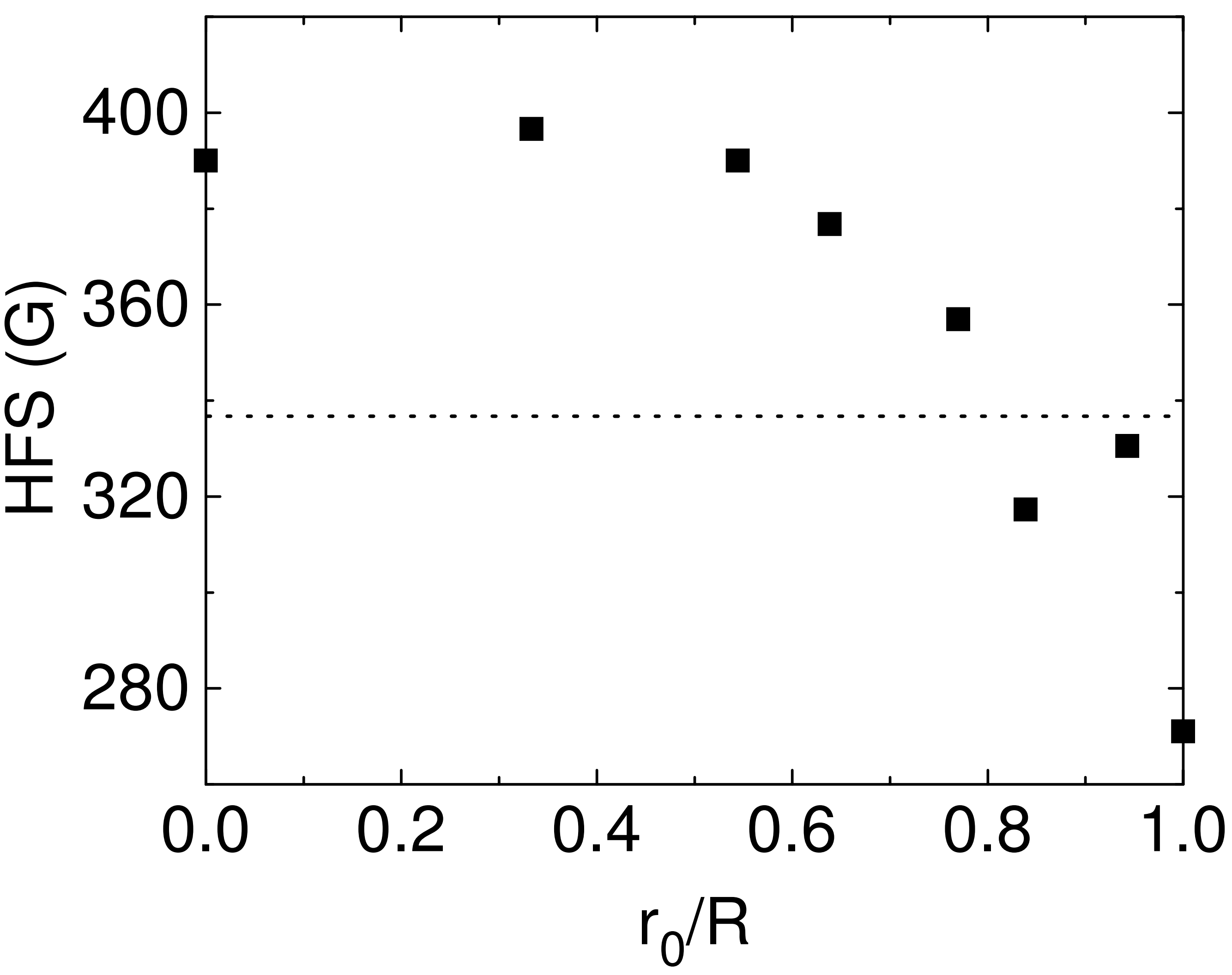
HFS (G)
400
360
320
280
0.0
0.2
0.4
0.6
0.8
1.0
r_0/R